CHALMERS
UNIVERSITY OF TECHNOLOGY

A significantly improved polymer||Ni(OH)<inf>2</inf> alkaline rechargeable battery using anthraquinone-based conjugated microporous

Materials Today Energy 27 (2022) 101014

Contents lists available at ScienceDirect

Materials Today Energy

journal homepage: www.journals.elsevier.com/materials-today-energy/

A significantly improved polymer||$Ni(OH)_2$ alkaline rechargeable battery using anthraquinone-based conjugated microporous polymer anode

Rebecca Grieco [a, d], Antonio Molina [a, d], Jaime S. Sanchez [a, b], Nagaraj Patil [a, **], Marta Liras [c], Rebeca Marcilla [a, *]

[a] Electrochemical Processes Unit, IMDEA Energy, Avda. Ramón de La Sagra 3, 28935 Móstoles, Spain
[b] Industrial and Materials Science, Chalmers University of Technology, Hörsalsvägen 7B, 41258, Göteborg, Sweden
[c] Photoactivated Processes Unit, IMDEA Energy, Avda. Ramón de La Sagra 3, 28935 Móstoles, Spain

ARTICLE INFO

Article history:
Received 29 March 2022
Received in revised form
5 April 2022
Accepted 6 April 2022
Available online 30 April 2022

Keywords:
Aqueous battery
Conjugated microporous polymer
Anthraquinone
Polymer electrode
Alkaline battery
Carbonyl porous polymers

ABSTRACT

Alkaline rechargeable batteries (ARBs) are predicted to be an attractive solution for large-scale electrochemical energy storage applications. However, their advancement is greatly hindered by the lack of high-performance and sustainable anode that can stably operate in less-corroding, low electrolyte concentration. Herein, we report the first example of polymer ARB able to operate in low concentrate electrolyte (1 M potassium hydroxide [KOH]) due to the employment of a robust anthraquinone-based conjugated microporous polymer (IEP-11) as anode. The assembled IEP-11||$Ni(OH)_2$ achieves high cell voltage (0.98 V), high gravimetric/areal capacities (150 mAh/g/7.2 mAh/cm^2 at 3.5 and 65 mg/cm^2, respectively), long cycle life (22,730 cycles, 960 h, 75% capacity retention at 20C), excellent rate performance (75 mAh/g at 50C) and low temperature operativity (75 mAh/g at −10 °C). Furthermore, rate capability, low-temperature performance and ability to prepare high mass loading anodes, along with low self-discharge is improved compared to conventional linear poly (anthraquinone sulfide) (PAQS) in commonly used 10 M KOH. This overall performance for IEP-11||$Ni(OH)_2$ is not only far superior to that of PAQS||$Ni(OH)_2$ owing to porous polymer's high specific surface area, combined micro-/mesoporosity and robust and mechanically stable three-dimensional (3D) architecture compared to the linear PAQS, but also surpass most of the reported organic||nickel [Ni]/cobalt [Co]/manganese [Mn] alkaline rechargeable batteries (ARBs).

1. Introduction

World's transition to a sustainable energy-based low-carbon society has created need for effective integration of electricity generated from renewable resources such as solar and wind power into batteries that are inexpensive, safe, environmentally benign, scalable and long lasting [1–3]. In this regard, aqueous rechargeable batteries (AqRBs) could offer tremendous competitiveness owing to their inherent advantages in terms of cost effectiveness, non-volatility, non-toxicity and non-flammability of water-based electrolytes [4,5]. Until now, numerous types of AqRBs such as Pb-acid, Zn-MnO_2, and Ni-based (e.g. Cd-Ni, Fe-Ni, Zn-Ni, metal hydride (MH)-Ni) have enjoyed great commercial success because of their safety and reliability aspects [6,7]. But they still fall short of meeting large-scale applications due to their low energy density, high self-discharge, memory effect, and most importantly, limited service life which imposes undesirable maintenance and frequent replacement of the batteries [4].

Most often, if not in all the cases, anode active-material has been the detrimental cycle-life-limiting component of these AqRBs. For instance, formation of a thick lead (II) sulfate ($PbSO_4$) passivation layer on Pb causes the premature aging of anode, resulting in poor cycle life of Pb-based acidic batteries [8]. Whereas, Ni-based alkaline rechargeable batteries (ARBs) that contain the same $Ni(OH)_2$ cathode but different anodes as stated above, suffer from either volume expansion/contraction during battery charge/discharge

* Corresponding author.
** Corresponding author.
E-mail addresses: nagaraj.patil@imdea.org (N. Patil), rebeca.marcilla@imdea.org (R. Marcilla).
[d] These authors contributed equally to this work.

https://doi.org/10.1016/j.mtener.2022.101014

cycling (in the case of metal hydride [MH] anode) [9] or poor deposition/dissolution coulombic efficiency by dendrite formation, hydrogen evolution, corrosion, and irreversible by-products formation (in the case of cadmium [Cd], iron [Fe], zinc [Zn] anodes), which once again negatively impact the cycle life of ARBs [5,10]. Therefore, it is still necessary to find robust anodes that are completely or partially free from the aforementioned drawbacks.

vEncouragingly, organic electrode materials (OEMs) have been proposed as suitable alternatives to the traditional metal anodes, since they store charge via an ion-coordination mechanism where material structure does not alter significantly over cycling [11–13]. Hence, they could achieve a much longer cycle life than those of their commercial counterparts. Advantageously, OEMs also exhibit greater natural abundance, less geopolitical constraints on resource availability, less toxicity, and can also be sometimes bio-based and biodegradable, which are in line with the sustainable battery development [14–16]. However, among a plethora of OEMs that have been successfully applied as electrodes in numerous rechargeable battery technologies, only quinone (particularly, 1,4-benzoquinone units), alloxazine and phenazine anodes were successfully evaluated in ARBs [17–23]. Unfortunately, due to solubility issues none of them have featured sufficient robustness to demonstrate the required longevity in the battery operation. To attain this requirement, dissolution of the active-material into the electrolyte has to be minimized by avoiding solubility of both the oxidized/reduced species in the selected alkaline electrolyte.

Since most of small OEMs are generally soluble in electrolytes, polymerization route has become one of the routine strategies to mitigate the dissolution issue by increasing the molecular weight of organic molecules [24–29]. Following the pioneering work by Nishide et al., in 2011 [30], many redox-active polymers (RAPs) containing densely populated 1,4-benzoquinodal moieties have been tested in alkaline electrolytes, but mostly assembled in polymer-air battery configuration [31–34]. Whereas, only a limited number of RAPs have been applied as organic anodes in combination with Ni/Co/Mn-based cathode in ARBs (see Table S1) [18–23]. But most notably, all these RAPs were non-porous linear polymers with insufficient robustness in alkaline electrolyte, thereby limiting the cycling stability. It is important to highlight that in all those examples a very high concentration of supporting base electrolyte (typically 10–13 M KOH) was necessary to mitigate the dissolution issues and to maintain sufficient cycle life. Therefore, the original objective of replacing problematic metal anodes in the well matured ARBs by a polymeric anode for a viable battery is still unmet.

Different from conventional linear RAPs, redox-active conjugated microporous polymers (RCMPs) are an emerging category of organic advanced materials that exhibit many intriguing properties such as high specific surface area, extended π-conjugation, permanent microporosity, and excellent physicochemical and thermal stability, which are appealing for their utilization as high performance OEMs in diverse electrochemical energy storage devices [35–40]. In this context, the robust and mechanically stable 3D microporous structure is one of the most appealing merit of the RCMP, anticipated to furnish advanced long-lived ARBs. Furthermore, their large specific surface area, delocalized π-conjugated long-range ordered skeleton, combination of micro-/mesoporosity and open channels are expected to enhance capability of fast charging and high-power densities, allowing full exploitation of the high ionic conductivity of aqueous alkaline media, which was quite neglected in the reported polymer ARBs. Despite exciting advances of RCMP-based organic electrodes in different energy storage technologies (e.g. supercapacitor [41–43], metal-ion [44–47], polymer-air [48], polymer-graphite [49] batteries, *etc.*), the implementation of RCMP anode in combination with Ni/Co/Mn-based cathodes for ARBs has not been explored.

Here we report on the use of anthraquinone-based conjugated microporous polymer/single-walled carbon nanotubes (SWCNTs) + reduced graphene oxide (RGO) hybrid material (named as IEP-11 for simplicity) as organic anode in combination with commercial $Ni(OH)_2$ cathode for advanced ARBs. This anode was found to exhibit ultrahigh performance in the commonly used high KOH concentrated electrolyte (*ca.*, 10 M), but more importantly and for the first time, also in alkaline electrolyte containing much lower KOH concentration (*ca.*, 1 M). Importantly, in addition to finding an appropriate RAP anode, electrolyte conditions also have to be optimized. Electrolyte, being another key component of the cell, lean electrolyte concentration while keeping its performance unimpaired has to be established for practical batteries [50]. Lower electrolyte concentrations not only reduce the cost of the battery, but also suppress oxygen evolution reactions on the $Ni(OH)_2$ cathode while charging, and mitigate both corrosion and self-discharge detrimental reactions [51,52]. These parasitic processes strongly affect the cyclability of $Ni(OH)_2$ cathode, and low electrolyte concentration would be beneficial to prolong the cycle life of the ARB.

The selection of IEP-11 hybrid is based on our previous works in which we demonstrated its outstanding electrochemical performance (high capacity utilization, high specific energy/power and ultralong cycling stability) in organic electrolytes for Li-ion batteries [44,45]. In this work, we systematically compare cycling, rate capability, low temperature performance, propensity to prepare high mass loading electrodes, self-discharge and float-charge characteristics of IEP-11 with the linear poly(anthraquinone sulfide) (PAQS)-one of the most applied organic anode in alkaline electrolyte (see Fig. 1a for chemical structure of polymers). All these electrochemical performance metrices for our anthraquinone-based conjugated microporous polymer hybrid (IEP-11) were not only remarkably superior to those for linear polyanthraquinone sulfide (PAQS), but also outperformed most of the reported organic||Ni/Co/Mn alkaline rechargeable batteries (ARBs). Most notably, IEP-11||$Ni(OH)_2$ in 1M KOH achieves high cell voltage (0.98 V), high anode specific capacity (150 mAh/g at 1C) and exhibits long cycle life (up to 22,730 cycles/960 h, with 75% capacity retention at 20C), excellent rate performance (75 mAh/g at 50C) and low temperature operativity (75 mAh/g at −10 °C).

2. Results and discussion

2.1. Synthesis and characterization of poly(anthraquinone) active-materials

Following the procedure described previously by us, the anthraquinone-based conjugated microporous polymer hybrid (named as IEP-11 for simplicity) was synthesized in two mini-emulsion and solvothermal steps from a mixture of monomers (2,6-dibromoanthraquinone and 1,3,5-triethynylbenzene) and carbon loading (5 wt.% of single-walled carbon nanotubes [SWCNTs] plus 5 wt.% of reduced graphene oxide [RGO]) through a Sonogashira cross coupling reaction [45]. Meanwhile, the linear poly (anthraquinone sulfide) (PAQS) was synthesized following the procedure reported elsewhere [18]. Brief synthetic protocol, including the schematics (Schemes S1 and S2) is given in the Supplementary Data.

The preliminary physicochemical characterization of the synthesized IEP 11 was carried out by routine analytical techniques. The detailed characterization was reported in our previous works [44,45], repeated here and briefly discussed in the Supplementary Data. Fourier-transform infrared (FTIR) spectroscopy and solid-

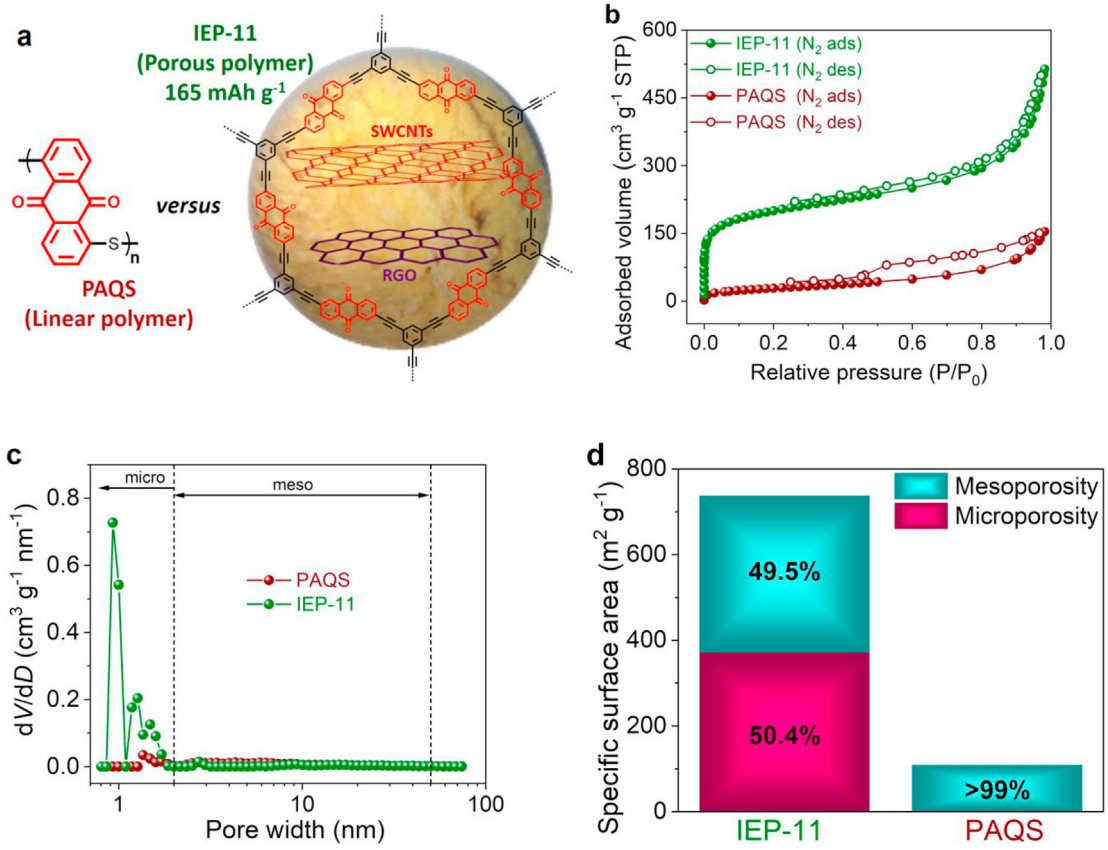

Fig. 1. Chemical structure of the reported polymers and their textural properties. a) Chemical structure of PAQS and idealized chemical structure of IEP-11. b) nitrogen adsorption–desorption isotherm profiles, c) pore-size distributions from the quenched solid density functional theory (QSDFT) model, and d) percentages of micro-/mesoporosity.

state ^{13}C nuclear magnetic resonance (NMR) spectroscopy confirm the chemical composition of the porous polymer, as represented in Fig. 1a, revealing successful incorporation of redox-active anthraquinone building blocks and triethynylbenzene linker (Figs. S1a and b). The presence of prominent G-band (1578 cm^{-1}) in the Raman spectrum affirm the integration of nanocarbons (SWCNT's and RGO) in the hybrid (Fig. S1c). Furthermore, intimate contact between the incorporated nanocarbons and polymer nanoparticles/nanowires can be visualized through transmission electron microscopy (TEM) imaging (Fig. S1d). Additionally, IEP-11 featured typical amorphous characteristics by X-ray diffraction (XRD) measurement (Fig. S1e), as expected for the porous polymer obtained through kinetically controlled Sonogashira coupling reaction [44]. Finally, thermal stability of IEP-11 was assessed by thermogravimetric analysis (TGA), revealing enhanced thermal stability up to 300 °C even under air (Fig. S1f).

In order to elucidate the textural properties of the poly (anthraquinone)s, nitrogen adsorption–desorption isotherm analysis was performed. Fig. 1b–d shows the relevant plots and Table S2 collects the extracted and calculated textural parameters from the isotherms. As previously demonstrated, in spite of the carbon content hybrid IEP-11 possess dual micro-/mesoporosity of 50.4/49.5%, wherein sharp contrast, linear PAQS was mainly characterized by the presence of mesopores (>99%) [44]. Furthermore, the Brunauer-Emmett-Teller (BET) specific surface area and total pore volume of IEP-11 was calculated to be 738 m^2/g and 0.7 cm^3/g, respectively, that are almost ~7- and ~3-fold larger than those of PAQS (104 m^2/g and 0.22 cm^3/g). Therefore, porous polymer features interesting improved textural parameters compared to its linear counterpart, which might be beneficial for enhancing the electrochemistry of porous active-material.

2.2. Electrochemistry of poly(anthraquinone) anodes in 1 M KOH

The electrochemical characterization of poly (anthraquinone) composite electrodes (~0.2 mg/cm^2 polymer mass loading) was carried out with cycling voltammetry (CV) in 1 M KOH using a standard three-electrode configuration. As shown in Fig. 2a and Fig. 2b, the CV profiles of PAQS/IEP-11 feature a pair of broad redox peaks around $E_{p,c}$ ~ −0.9/−0.93 V (vs. Hg/HgO) and $E_{p,a}$ ~ −0.7/−0.68 V corresponding to the reduction (and potassiation) and oxidation (and de-potassiation) reactions of anthraquinone and anthraquinolate anion units, respectively. Being consistent with the previous reports (*vide supra*), this suggests that anthraquinone/anthraquinolate moieties are responsible for the observed redox activity in both the polymers, and they experience similar redox chemical microenvironment. Interestingly, upon repeated cycling over 100 cycles, there was a visible decrease in peak current intensity for PAQS, and the decrease of the same for IEP-11 was negligible. Apparent coloration of the electrolyte for PAQS (see inset in Fig. 2a) indicates that the decrease in peak currents was due to the dissolution of active material into the electrolyte, while no such coloration has been observed for IEP-11, inferring that the anthraquinone building blocks exhibit improved dimensional stability in IEP-11 than in PAQS. Complementing the CV results, it can also be seen from galvanostatic charge–discharge (GCD) experiments that, IEP-11 demonstrate enhanced cycling stability (92 vs. 59% of its initial capacity retention over 500 cycles) than PAQS (Fig. 2c and Fig. S2). The stability of these polymeric active-materials will be discussed in detail in later section.

Furthermore, GCD experiments were extended to study rate capability of poly (anthraquinone) composite electrodes at

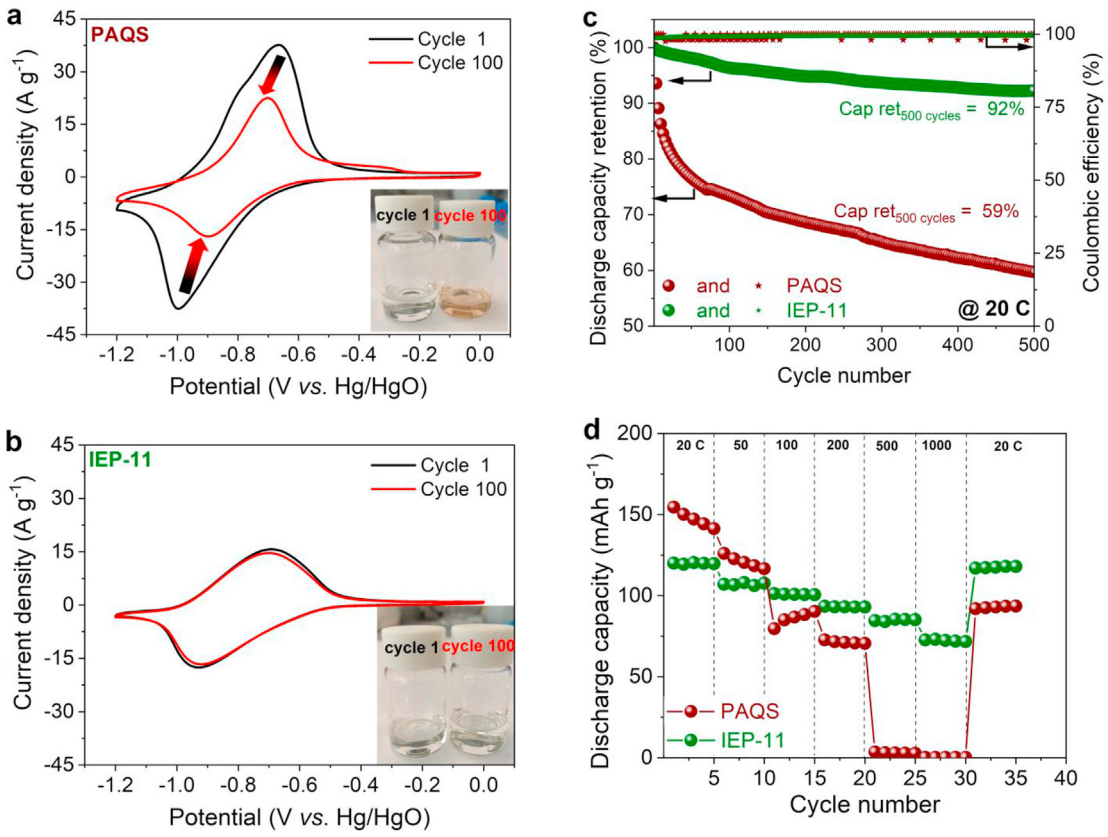

Fig. 2. Electrochemical performance of PAQS and IEP-11 in three-electrode configuration. Set up: polymer deposited on carbon paper (~0.2 mg/cm^2), Hg/HgO and Pt mesh as the working, reference and counter electrodes, respectively, in 1 M KOH aqueous electrolyte. a, b) Successive cyclic voltammograms of PAQS (a) and IEP-11 (b) for 100 cycles obtained at 20 mV/s. Inset shows the coloration of electrolyte solutions after the CV measurement. c) Cycle stability by GCD experiment: discharge capacity retention and Coulombic efficiencies measured at 20C. d) Rate capability: discharge capacity vs. cycle number at various C-rates.

different current rates (C-rates), ranging from 20C to 1000C (1C = 224 and 165 mAh/g for PAQS and IEP-11, respectively). It is clearly evident from Fig. 2d that specific capacity values for IEP-11 at higher C-rates decreased to a small extent compared to the capacity at 20C, whereas, the loss of capacity was significant in the case of PAQS. For instance, the capacity retention was 78% for IEP-11 vs. only 47% for PAQS at 200C (Fig. S3). In noteworthy manner, IEP-11 still delivered a remarkable capacity of 72 mAh/g at an extremely high C-rate of 1,000C, that corresponds to 61% of capacity retention compared to the value at 20C, but PAQS was almost non-functioning at this C-rate.

We investigated this improved rate performance for IEP-11 over PAQS in detail by cycling voltammetry (CV), electrochemical impedance spectroscopy (EIS) and galvanostatic intermittent titration techniques (GITTs). All the important electrochemical and transport properties parameters are collected in Table S3 and discussed in detail in the. First, the EIS measurement of poly (anthraquinone)||activated carbon cells were carried out at different temperatures (from +25 to −15 °C). All the Nyquist plots feature two well-defined regions: a depressed semicircle in the high frequency region and an inclined line in the low-frequency that provide information about the charge-transfer resistance (R_{ct}) and diffusion of K^+ ions in the bulk of the electrode, respectively, which are connected by Warburg impedance (σ_w), represented by a line of ~45 degrees slope (Fig. S4) [53]. At the given temperature, IEP-11 exhibited lower R_{ct}, and also its increment was minute with decrease of temperature than that of PAQS (Fig. S5). Furthermore, this temperature dependence of R_{ct} was exploited to determine an activation energy (E_a) parameter, calculated using the negative slope of Arrhenius plots (Fig. 3a). It was found that, the E_a for IEP-11 was significantly lower than that of PAQS (5.9 vs. 9.4 kJ/mol). Akin to the trend in R_{ct}, similar tendency in σ_w has been observed (Fig. S6). As σ_w is inversely proportional to the ion diffusivity, a higher ionic conductivity thus expected for IEP-11 over PAQS. Subsequently, K^+ diffusivity was determined by GITT measurement at +25 °C (Fig. S7). In general, K^+ diffusivity at all the open circuit voltages (OCVs) was higher for IEP-11 than for the PAQS, with an average value of 19 vs. 8.2 $\times$ 10^{-7} and 14 vs. 9.1 $\times$ 10^{-7} cm^2/s (IEP-11 vs. PAQS) for charging and discharging cycles, respectively (Fig. 3b), thus corroborating EIS results of higher ionic conductivity in the bulk of the electrode in IEP-11 > PAQS order.

Second, the CV experiments at various scan rates (v) were carried out to determine kinetic parameters, heterogeneous reaction rate constant (k^0) and transfer coefficient (α) from the v-dependence of the peak potentials using the Laviron method [54]. At the given v, the CVs of IEP-11 were characterized by a smaller peak-to-peak potential separation than that of PAQS (Fig. 3c and d), suggesting faster redox kinetics in the former case. Quantitatively, k^0 for IEP-11 was calculated to be about 80-fold higher than that of PAQS (56 vs. 0.7/s; Fig. 3e and f). Considering the physical significance of k^0, the redox system with the higher k^0 reaches reaction equilibrium faster owing to the lower activation energy (Fig. 3a), faster ion-mobility (Fig. 3b), and thus, facilitated redox kinetic (Fig. 3c–f). Also, the value α was close to 0.5 for IEP-11 than that of PAQS ($\alpha = 0.4$) suggesting that more symmetric energy barriers for the oxidation and reduction reactions were accounted in the case of IEP-11.

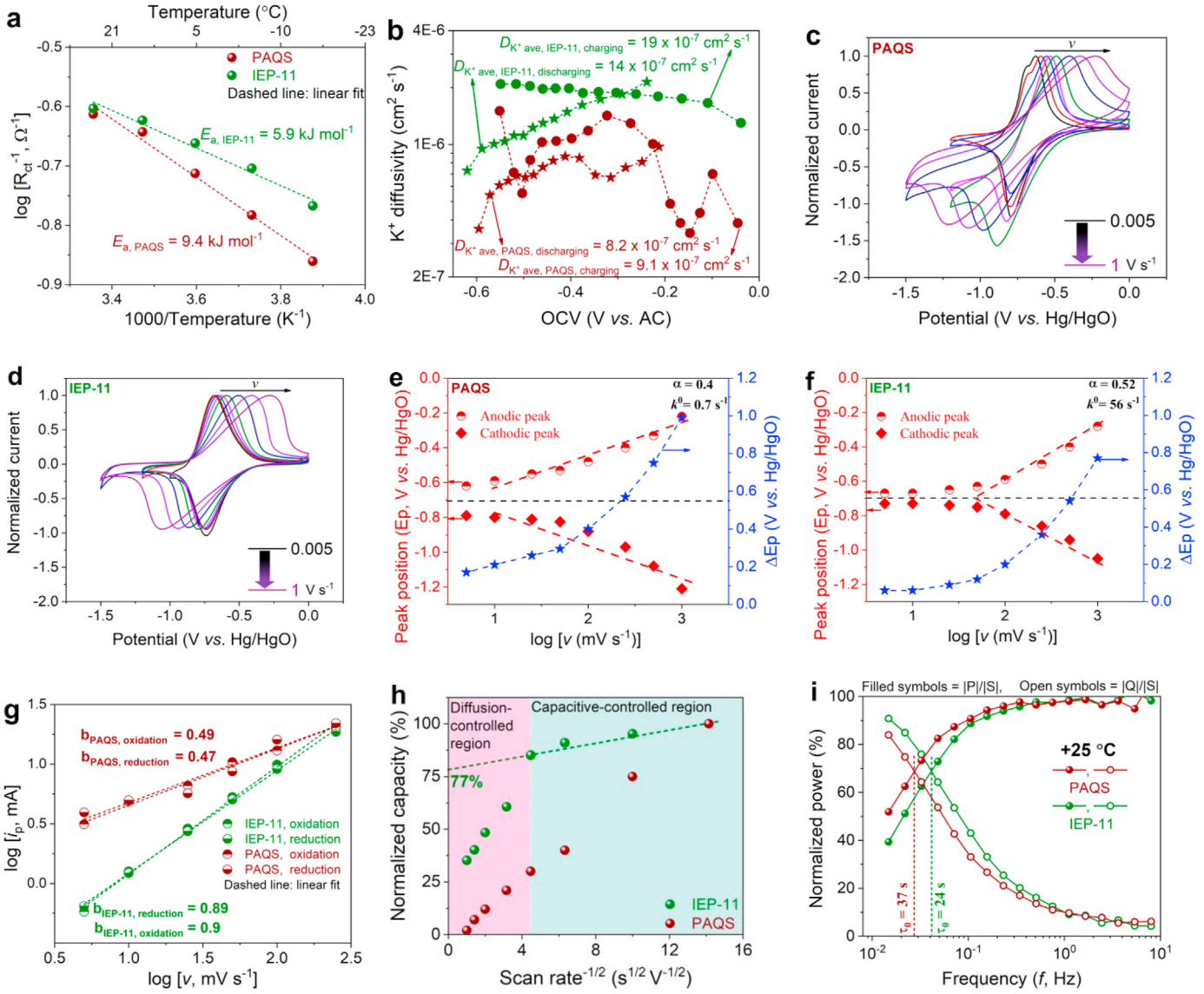

Fig. 3. Comparative electrochemical kinetic evaluation of PAQS and IEP-11 in 1 M KOH electrolyte. a) A fitting of temperature dependence of charge-transfer resistance with the Arrhenius equation to calculate activation energy. b) Ion diffusivity calculated from GITT measurement as a function of OCV. c, d) CVs at different scan rates. The CVs are normalized by the peak anodic current to show the peak shift with the scan rates. e, f) Laviron plots: indicating the variation of anodic and cathodic peak positions (Ep), and ΔEp as a function of the scan rate (in logarithmic scale). g) Peak current vs. scan rate in logarithmic scale to obtain b-values according to $i_p = av^b$. h) Normalized capacity vs. scan rate$^{-1/2}$ plots allow the quantification of diffusion-controlled and capacitive-controlled capacity contributions to the total stored charge. i) Complex power analysis plot at +25 °C. The crossing of the normalized |*P*|/|*S*| and |*Q*|/|*S*| plots corresponds to the relaxation time constant τ_0.

Then, the CV analysis was further extended to obtain power-law behavior of these polymeric active-materials: peak currents (i_p) vs. v that obeys $i_p = av^b$ relationship, where, a and b are adjustable coefficients [55]. The exponential b-value can be determined by the slope of log (i_p) vs. log (v) plot for the redox processes. Ideally, the b-value of 0.5 indicates a diffusion-controlled process, whereas the b-value of 1.0 is the signature of a capacitive-controlled behavior. A high b-value of 0.89/0.9 for IEP-11 vs. 0.47/0.49 for linear PAQS for the reduction/oxidation peaks (Fig. 3g), specify that overall redox response tends to be more capacitive-controlled in the case of IEP-11. On the contrary, a lower b-value (close to 0.5) suggests that the redox processes are more diffusion-controlled for PAQS. Here, the capacitive-type electrochemical response for IEP-11 is assumed to have mainly originated from bulk electrochemical reaction sites that are less limited by the diffusion processes on account of polymer's intrinsic high specific surface area and micro-/mesoporosity, rendering high reaction rates and superior ion mobilities [44]. Specifically, we further quantified the contributions of diffusion- and capacitive-controlled charge storage to the total capacity by applying the correlation between normalized capacity and $v^{-1/2}$ that give us the quantitative assessment of the electrode's rate capability (See ESI for details) [55]. From Fig. 3h, two regions are evident for IEP-11: in the diffusion-controlled region, the capacity decreases strongly with increasing the v, whereas charge contributions in the capacitive-controlled region demonstrated a small dependency on the v. Therefore, 77% of the total capacity for IEP-11 was capacitive-controlled below 20 mV/s, wherein contrast, a linear dependency of capacity on the $v^{-1/2}$ throughout the tested v range was observed for PAQS suggesting that most of the capacity delivery was controlled by the diffusion processes in PAQS.

This enhanced capacitive behavior for IEP-11 over PAQS was further substantiated by electrochemical impedance spectroscopy

(EIS) analysis. The maximum attainable impedance phase angle (−θ) at 10 mHz for IEP-11 was higher than that of PAQS at all the temperatures (Fig. S8 and associated text). Higher the −θ, larger the capacitive contribution. Relaxation time constant (τ_0) that defines the frontier between the resistive and the capacitive behavior determined by complex power analysis (see Fig. S9 and associated text for the description of τ_0), was found to be lower for IEP-11 than that of PAQS at all the temperatures. The lower τ_0 value is associated with the faster delivery of the stored energy [54].

Taken together, all these electrochemical enhancement parameters should impart superior dynamic behavior to the porous polymer over its linear analog.

2.3. Construction of poly(anthraquinone)||Ni(OH)$_2$ alkaline rechargeable battery

Owing to reasonably low redox potential of poly (anthraquinone), i.e. −0.7 V (vs. Hg/HgO) and relatively high redox potential of $Ni(OH)_2$, i.e. +0.42 V (vs. Hg/HgO), a full cell with an optimal average output voltage of just over a volt can be constructed in basic electrolyte medium. Fig. 4a shows a schematic illustration of the full cell structure and the overall electrode reactions of the cell in KOH is also given. This battery operates in a non-rocking chair dual-ion configuration with K^+/OH^- electrolyte ions: during the charge process, $2OH^-$ from the electrolyte are inserted into the $Ni(OH)_2$ cathode, while oxidizing it to NiO(OH), and simultaneously releasing electrons into the external circuit. While at the polymer anode, anthraquinone units are reduced by gaining electrons from the external circuit to the anthraquinolates with the uptake $2K^+$ ions per anthraquinone unit from the electrolyte. Conversely, anthraquinolates are oxidized to anthraquinones, and the NiO(OH) is reduced to $Ni(OH)_2$ with the concomitant reversible break away of $2K^+$ and $2OH^-$ and return to the electrolyte from the anode and cathode active sites, respectively, during the discharge process.

Interestingly, the cell voltage of a poly(anthraquinone)||$Ni(OH)_2$ battery depends on the pH, which is related to the concentration of the KOH electrolyte [56]. To demonstrate this, the CV (glassy carbon modified electrodes) of full cell and its individual electrode partners were recorded in three different KOH concentrations, i.e. 1, 5 and 10 M of pH 13.8, 14.5, and 15.7, respectively (Fig. 4b). Since poly (anthraquinone) operates above the pK_a value of aromatic hydroxyl groups (pK_{a1} ≈ 9 and pK_{a2} ≈ 12) [23] in all these electrolytes, it did not exhibit pH dependent peak shift. On the contrary, since hydroxide ions participate in the redox reaction of $Ni(OH)_2$, an increase in the $[OH^-]$ i.e. increase of pH causes a shift in the redox potential of the cathode towards more negative values. In order to maximize the cell voltage, the potential of the anode and the cathode should be kept as low (negative) and as high (positive) as possible, respectively. Thanks to the distinguishing voltage characteristics of poly (anthraquinone) and $Ni(OH)_2$, full cells with increasing voltage output of 0.96, 1.05, and 1.1 V in 10, 5, and 1 M KOH, respectively, can be anticipated. This hypothesis was further confirmed with more practical batteries (polymer mass loading above 3.5 mg/cm^2) from GCD profiles, revealing +90 mV and +130 mV increment in 1 M KOH for PAQS and IEP-11 anodes, respectively, compared to the same system in 10 M KOH (Fig. S10 and associated text). Therefore, lower KOH electrolyte concentration, for instance, 1 M favors to achieve the highest cell voltage of 0.98 V for IEP-11||$Ni(OH)_2$ battery. On account of this voltage gain in 1 M KOH, IEP-11||$Ni(OH)_2$ attained an enhanced specific energy of 132.5 (versus 127.6) Wh/kg$_{anode}$, even though the IEP-11 anode realized a slightly higher specific capacity of 150 mAh/g (+15 mAh/g) in 10 M KOH.

2.4. Comparative electrochemical performance of PAQS||Ni(OH)$_2$ and IEP-11||Ni(OH)$_2$

PAQS||$Ni(OH)_2$ and IEP-11||$Ni(OH)_2$ full cells were assembled (see experimental section in Supplementary Data for the electrode preparation and cell assembly) using mainly 1 M KOH aqueous electrolyte, and 10 M KOH was also employed, whenever necessary. Their electrochemical performance, cycle-life, rate capability, low-temperature operativity, self-discharge, etc. was evaluated by galvanostatic charge-discharge (GCD) experiments.

2.4.1. Cycle-life assessment

The cycling stability of PAQS||$Ni(OH)_2$ and IEP-11||$Ni(OH)_2$ cells in 1 M KOH was compared at 1 and 20C. At a low C-rate of 1C, IEP-11||$Ni(OH)_2$ attained stable capacities quickly, and impressively retained 76% of its initial capacity over 2,000 repeated full charge/discharge cycles (Fig. S11). On the contrary, capacity decay was very drastic in the case of PAQS||$Ni(OH)_2$ that only retained 34% of its initial capacity over 500 cycles. More strikingly, when IEP-11||$Ni(OH)_2$ was cycled at high operational rate of 20C, the cell demonstrated an ultralong life-span; sustaining reversible capacity at 85 mAh/g with a remarkable capacity retention of 75% after

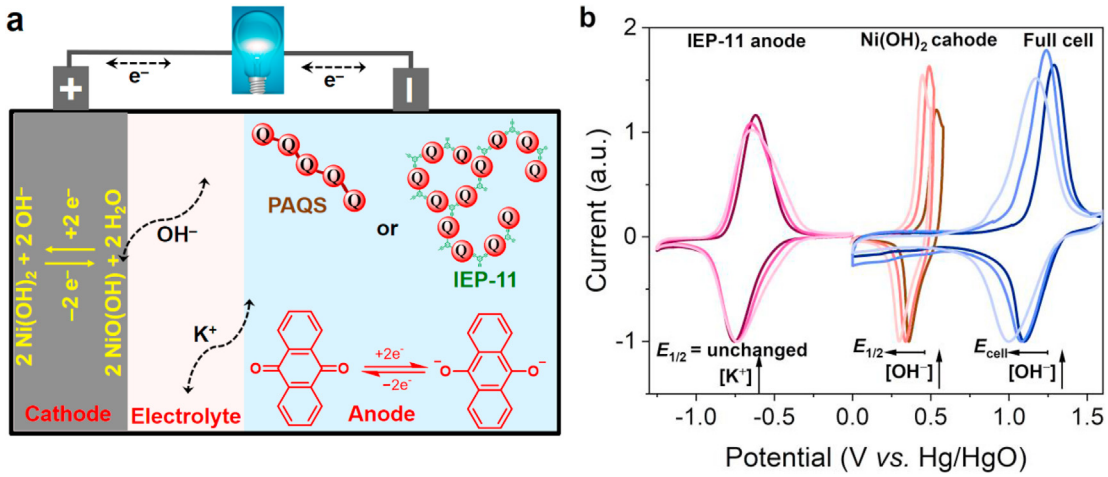

Fig. 4. Construction of poly(anthraquinone) || Ni(OH)$_2$ alkaline rechargeable battery. a) Schematic of full cell and its working mechanism, and b) CVs of IEP-11 and $Ni(OH)_2$ in three-electrode configuration with active-material modified glassy carbon (GC), Hg/HgO and Pt mesh as the working, reference and counter electrodes, respectively, and full cell in 1, 5 and 10 M KOH.

extended 22,730 cycles, losing a minute 0.0012 mAh/g/cycle or 0.7 mAh/g/day (total cycling period of 40 days) (Fig. 5a and Fig. S12). While at this C-rate, PAQS||$Ni(OH)_2$ once again retained merely a 35% capacity over 6,240 cycles. It is also worth to mention here that after initial few activation cycles (particularly, with polyanthraquinone sulfide [PAQS]), the average Coulombic efficiencies in all of the cycling tests remained above 99%.

As previously pointed out by other researchers, the capacity decay in the case of linear polymers (e.g. PAQS) in dilute basic electrolytes is due to the dissolution of reduced species into the aqueous solution. This observation is also exemplified in our controlled experiments (Fig. S13). When the PAQS||$Ni(OH)_2$ cell was immediately discharged after full charge, it lost 49% of the charge capacity in the first cycle. The loss of first cycle charge capacity further increased when the full cells were held for 5 h rest and 2 h float charge (constant voltage charge) in the charged state, which resulted in only 24 and 20% charge capacity retention, respectively. Wherein contrast, the loss of first cycle charge capacity in the case of our IEP-11||$Ni(OH)_2$ in all these different protocols was almost negligible, demostrating robustness of 3D porous polymer structure to avoid the dissolution of reduced species into the electrolyte.

Supplementing the half-cell studies by cycling voltammetry (CV), *post mortem* analysis of the cycled full cells revealed similar coloration phenomenon. The Whatman separator, recovered from PAQS|1 M KOH|$Ni(OH)_2$ cell showed full of reddish brown coloration, whereas, the same from IEP-11|1 M KOH|$Ni(OH)_2$ was colorless (Fig. S14a). Field-emission scanning electron microscopy (FE-SEM) analysis of the cycled PAQS electrode revealed decreased surface roughness (originated from randomly embedded polymer particles in the pristine electrode) [57] with sparse active-material coverage on the electrode that can be seen from the exposed carbon additives upon cycling, accompanied by increased porosity or void formation possibly due to the dissolution of polymer into the electrolyte (Figs. S15a–f). This dissolved polymer passed across the separator and deposited on the $Ni(OH)_2$ side as indicated by its surface smoothening (loss of granular/scaly open morphology of pristine electrode; Figs. S16a and c) and field emission scanning electron microscopy (FE-SEM)/ energy dispersive X-ray spectroscopy (EDS) mapping (increased C intensity and found traces of S; Fig. S17), leading to an irreversible self-discharge. On the contrary, the intrinsic porosity (Figs. S18a–f) and granular/scaly open surface morphology (Figs. S16e and f) of the pristine IEP-11 and $Ni(OH)_2$ electrodes, respectively, was intact without significant changes, and no signature of IEP-11 deposits on the $Ni(OH)_2$ observed in the case of IEP-11|1 M KOH|$Ni(OH)_2$ cycled subsequently. (Fig. S19).

Furthermore, in our studies, we also found that PAQS||$Ni(OH)_2$ in 10 M KOH (that typically used to circumvent dissolution issues) demonstrated similar capacity decay, but definitely improved compared to the cycling in 1 M KOH (Fig. S20). The Whatman separator, recovered from the above cell was still colored (Fig. S21a), and FE-SEM/EDS mapping inferred similar observations as in 1 M KOH (Fig. S15g–i, S16e and S22a). No such solubility detrimental effects have been observed for IEP-11||$Ni(OH)_2$ in 10 M KOH (Fig. S16f, S18g–i, S21b and S22b).

2.4.2. Rate capability assessment

Fig. 5b–e show the comparative rate performance of PAQS||$Ni(OH)_2$ and IEP-11||$Ni(OH)_2$ cells in 1 M KOH by galvanostatic charge-discharge (GCD) studies at progressively increasing C-rates with the representative specific capacity–voltage profiles depicted in Fig. 5b and c. At a low C-rate of 1C, PAQS||$Ni(OH)_2$ delivered a low reversible discharge capacity of 60 mAh/g (27% capacity utilization). Interestingly, IEP-11||$Ni(OH)_2$ demonstrated higher discharge capacity of 150 mAh/g with 91% capacity utilization. Additionally, with increasing C-rates, both the capacities (Fig. 5d) and consequently their capacity retentions (Fig. 5e) decreased monotonically in IEP-11 < PAQS order. For instance, the discharge capacities (and their percent retentions) at a high C-rate of 50C were 25 (34%) and 90 (63%) mAh/g for PAQS||$Ni(OH)_2$ and IEP-11||$Ni(OH)_2$, respectively. Even at an extreme C-rate of 500C, IEP-11||$Ni(OH)_2$ still registered considerable capacity of 20 mAh/g, while PAQS||$Ni(OH)_2$ was almost non-functioning. Furthermore, when the C-rate was brought back to 1C, nearly quantitative capacity recovery was observed in the case of IEP-11||$Ni(OH)_2$, signifying a strong tolerance to the rapid K^+/OH^- ions insertion/removal reactions. Whereas, incomplete capacity recovery at 1C was noted with PAQS||$Ni(OH)_2$, probably due to the irreversible capacity losses, associated with the PAQS dissolution issues.

We further enhanced the rate capability of full cells by employing 10 M KOH that exhibits superior ion transport properties compared to than in 1 M (Fig. S23) [58]. Though capacity values were improved for PAQS||$Ni(OH)_2$ compared to those in 1 M KOH, the enhancement in rate capability was not very significant. But in the case of IEP-11|10 M KOH|$Ni(OH)_2$ there was at least 4x and 3.5x times rate enhancement with higher capacity values of 81 and 49 mAh/g (versus 20 mAh/g and 14 mAh/g) at extreme C-rates of 500C and 1000C, respectively, compared to the same in 1 M KOH.

2.4.3. Low-temperature performance

It is necessary to develop advanced batteries for some special applications, such as polar inspections, high-altitude drones, and aerospace that work reasonably under these extreme conditions of low temperatures [59]. Most often, aqueous electrolytes will freeze at subzero temperatures, resulting in device failure [60]. Besides, the increased charge transfer resistance, and the sluggish kinetics of the electrodes at low temperatures limits their capacity utilization and rate performance.

One of the advantages of alkaline aqueous electrolytes is their low freezing temperature compared to the neutral counterparts. We exploited this advantage of 1 and 10 M KOH aqueous solutions to evaluate low-temperature rate performance of PAQS||$Ni(OH)_2$ and IEP-11||$Ni(OH)_2$ cells at different temperatures, ranging from +25 to −40 °C. IEP-11||$Ni(OH)_2$ in 1 M KOH delivers discharge capacities of 110, 105, 103, 99 mAh/g and 100, 95, 90, 83 mAh/g at 2C and 20C, respectively, and at the operational temperatures of +25, +10, 0, and −10 °C, respectively, vs. lower capacities of 81, 72, 61, 50 mAh/g and 58, 51, 35, 0 mAh/g for PAQS||$Ni(OH)_2$ (Fig. 5f and Fig. S24). Indeed, IEP-11||$Ni(OH)_2$ not only achieved higher capacities at all the C-rates, but their retention, for instance, at 2C and 20C, at lower temperatures (compared to the capacity value at +25 °C) were also superior to that of PAQS||$Ni(OH)_2$ (Fig. S25). Additionally, low-temperature operativity of these cells was further improved beyond −10 °C by employing more concentrated KOH aqueous electrolyte (ca. 10 M). Despite capacities of PAQS||$Ni(OH)_2$ in 10 M KOH were boosted to higher values (compared to that in 1 M KOH), their retention at lower temperatures and higher C-rates was similar to that in 1 M KOH (Figs. S26 and S27). In other words, at rather low temperatures of −20, −30, and −40 °C, and at a high C-rate of 20C, IEP-11||$Ni(OH)_2$ remarkably sustain high capacities of 86, 78, 63 mAh/g vs. lower 68, 58, 33 mAh/g for PAQS||$Ni(OH)_2$, that correspond to extraordinary 79, 71, 57% vs. inferior 59, 50, 28% capacity retention compared to the capacity at +25 °C (Fig. S26c). Moreover, after low-temperature rate performance experiments, when the operational temperature was reset back to +25 °C, the capacities of IEP-11||$Ni(OH)_2$ in both 1 and 10 M KOH electrolytes were almost recovered to their initial values, suggesting negligible intolerance of cell components towards the low-temperature. Where on the contrary, partial capacity recovery in the case of PAQS||$Ni(OH)_2$, once again highlights low-temperature-resilient characteristic of our porous polymer over linear one.

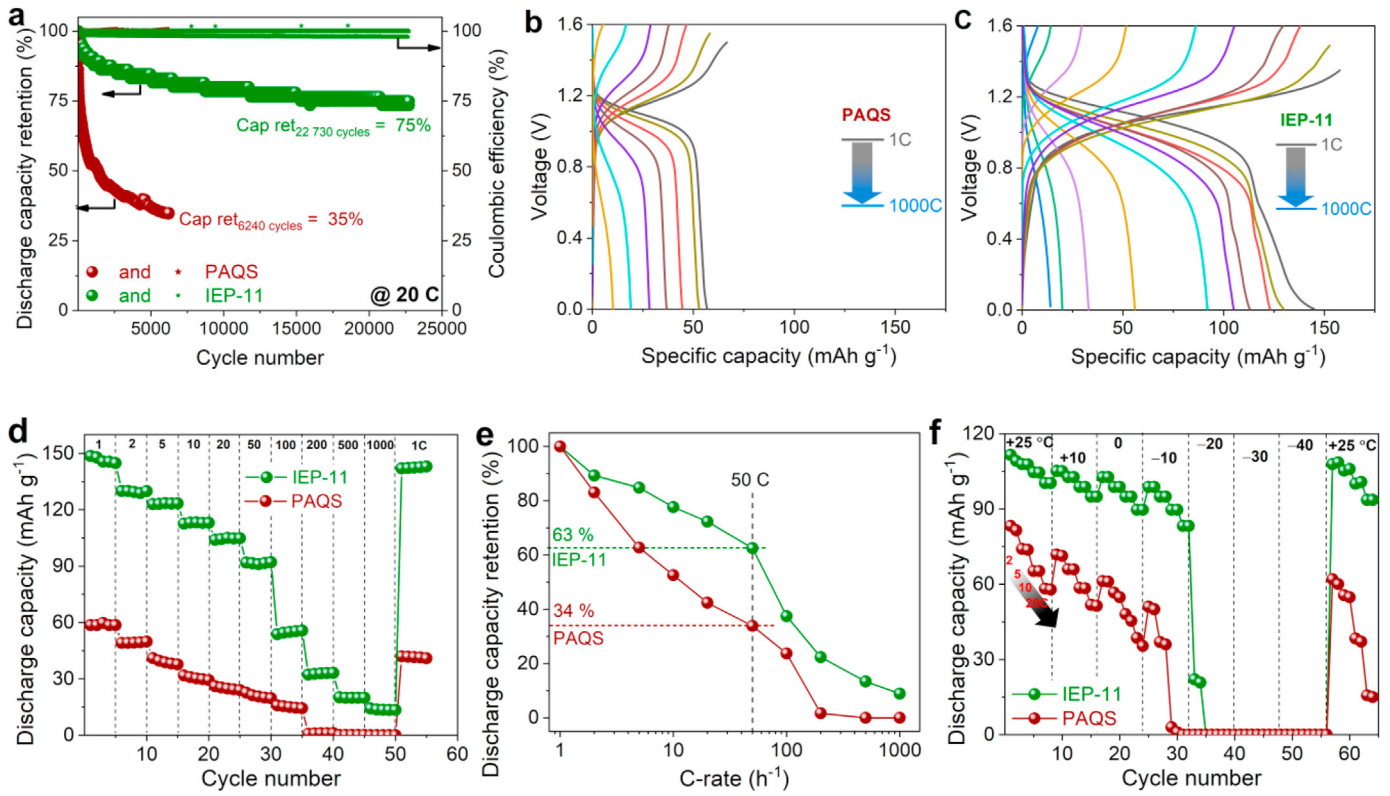

Fig. 5. Comparative electrochemical performance of PAQS || $Ni(OH)_2$ and IEP-11 || $Ni(OH)_2$ full cells in 1 M KOH. a) Cycle stability: discharge capacity retention and Coulombic efficiencies measured at 20C. b–e) Rate capability: representative specific capacity–voltage profiles at various C-rates for PAQS || $Ni(OH)_2$ (b) and IEP-11 || $Ni(OH)_2$ (c), discharge capacity vs. cycle number at various C-rates (d), and discharge capacity retention at different C-rates (e). The discharge capacities at higher C-rates are normalized with respect to the discharge capacity at 1C. f) Low-temperature operativity: Discharge capacity vs. cycle number, recorded at different C-rates (from 2C to 20C) and at different temperature (from +25 °C to −40 °C).

2.4.4. Alkaline polymer//$Ni(OH)_2$ battery with high mass Loading polymer anodes

Inspired by the superior electrochemical performance of IEP-11 over PAQS with the polymer mass loading used in previous section (typically, below 3.5 mg/cm^2), we were stimulated to prepare even higher mass loading anodes, targeting at further boost the capacity values at the electrode level. For practical applications, it is of paramount importance to develop thick electrodes (areal capacities beyond 3°mAh/cm^2) in order to fully exploit the cost advantages of high mass loading sustainable electrodes [61]. We adapted bucky-paper approach to construct different mass loading polymer anodes from ~2 to ~65 mg/cm^2 (see Fig. S28 for their digital images). Also, 10 M KOH was used to study the intrinsic electrochemical characteristic of polymers (particularly, PAQS that has solubility issues in 1 M KOH), and in the end is compared with 1 M KOH as well.

Comprehensive electrochemical performance evaluation of PAQS||$Ni(OH)_2$ and IEP-11||$Ni(OH)_2$ cells in 10 M KOH having different polymer mass loadings in the anode was carried out through GCD experiments at different C-rates (Fig. S29 and S30a, b) or areal currents (Fig. 6 and Fig. S30c, d). The representative areal capacity–voltage profiles at 0.5C and 15C are also shown in Fig. S31. Fig. 6a and b show the gravimetric/areal capacities of PAQS||$Ni(OH)_2$ and IEP-11||$Ni(OH)_2$, respectively, with various polymer mass loadings in the anode at low C-rate (0.5C). The areal capacity for IEP-11||$Ni(OH)_2$ scaled almost linearly with the mass loading below 10 mg/cm^2 due to its superior mass utilization (>95%; Fig. 6c), and thus, near-theoretical gravimetric capacity (165 mAh/g) values were attained. While significant deviation in areal/gravimetric capacity was observed in the case of PAQS||$Ni(OH)_2$, particularly at higher mass loadings (above 5 mg/cm^2). For instance, at a high polymer mass loading of 62 mg/cm^2 and 65 mg/cm^2 for PAQS and IEP-11, respectively, IEP-11||$Ni(OH)_2$ still maintained very high gravimetric capacity of 117 mAh/g vs. 110 mAh/g for PAQS||$Ni(OH)_2$, which implies an exceptional 71 vs. mediocre 49% anthraquinone mass utilization in IEP-11 vs. PAQS. Consequently, IEP-11||$Ni(OH)_2$ was able to achieve the highest areal capacity of 7.6 vs. 6.8 mAh/cm^2 for PAQS||$Ni(OH)_2$ at these high mass loadings, despite higher theoretical specific capacity for the latter (224 mAh/g).

Fig. 6d–f depict the rate capability of PAQS||$Ni(OH)_2$ and IEP-11||$Ni(OH)_2$ cells with low (~2 mg/cm^2), intermediate (~10 mg/cm^2) and high (~65 mg/cm^2) polymer mass loading anodes, respectively. The areal/gravimetric capacities and their retention decreased unvaryingly with increasing both the polymer mass loadings and the areal currents/C-rates. But this decrease was more propound with higher mass loading electrodes, especially at higher currents, relatively in the case of PAQS over IEP-11. It is remarkable that IEP-11||$Ni(OH)_2$ still achieved an extraordinary areal capacity of 3.4 mAh/cm^2 (vs. 0.62 mAh/cm^2 for PAQS||$Ni(OH)_2$) at the high C-rate of 5C with the highest mass loading anodes (Fig. S30b). Even more strikingly, the aforementioned IEP-11||$Ni(OH)_2$ cell was able to be charged (or discharged) only within ~0.01 h, still maintaining high areal capacity values at 1.25 mAh/cm^2 (Fig. 6f) and sustaining a large areal current density as high as 340 mA/cm^2 (or 15C ≈ 5.2 A/g) demonstrating its suitability as 'ultrafast battery'. Whereas, PAQS||$Ni(OH)_2$ cell was non-functional under these severe testing conditions.

The feasibility of obtaining high mass loading electrodes of IEP-11 still achieving excellent electrochemical properties can be seen from similar studies but in 1 M KOH (Figs. S31–S33). Owing to the

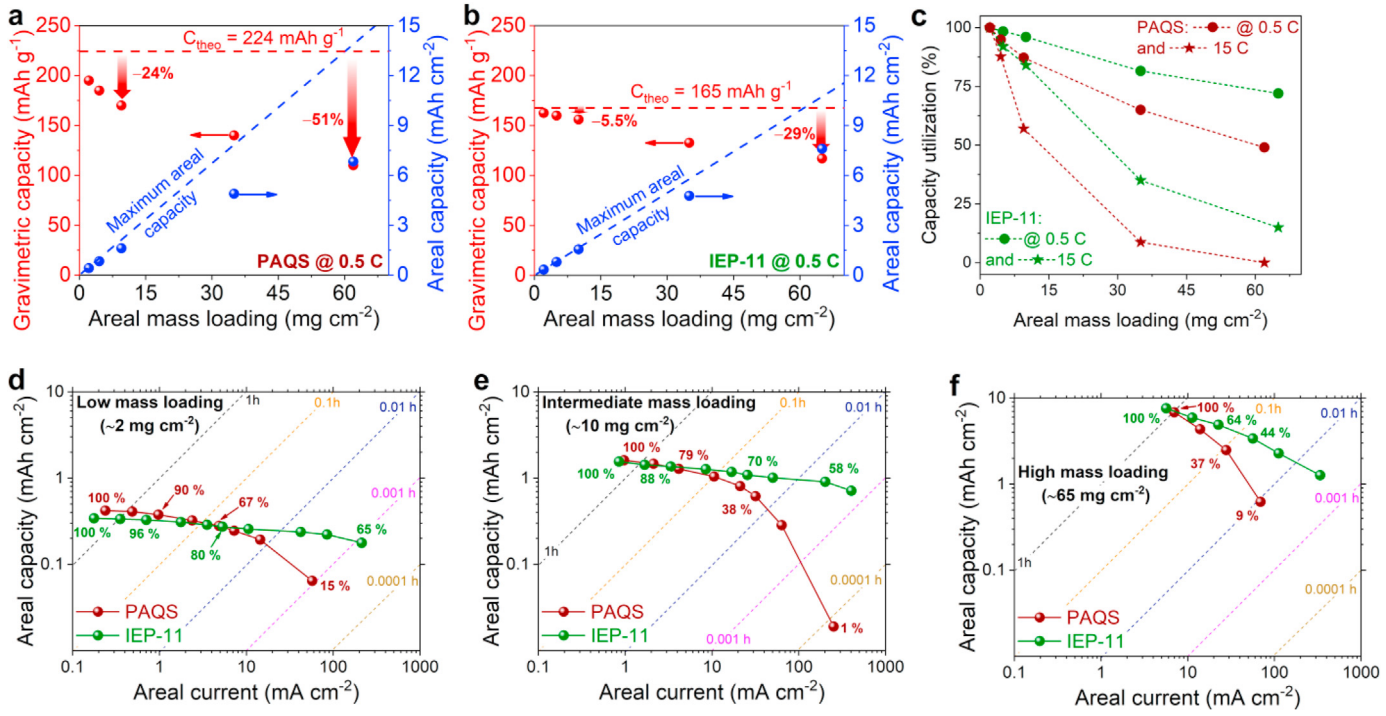

Fig. 6. Comparative electrochemical performance of PAQS || $Ni(OH)_2$ and IEP-11 || $Ni(OH)_2$ full cells at different polymer mass loadings in the anode in 10 M KOH. a–c) Gravimetric/areal capacities of PAQS || $Ni(OH)_2$ (a) and IEP-11 || $Ni(OH)_2$ (b), and capacity utilization at 0.5 and 15C as a function of mass loading. d–f) Rate capability: areal capacities as a function of areal current for low (~2 mg/cm^2; d), intermediate (~10 mg/cm^2; e) and high (~65 mg/cm^2; f) mass loading anodes.

dissolution issues of PAQS in 1 M KOH, the capacity utilization, and thus, gravimetric capacities of PAQS||$Ni(OH)_2$ with low (3.5 mg/cm^2) and high (65 mg/cm^2) mass loading polymer anodes were greatly reduced (below 30% and as low as 60 mAh/g; Fig. S32). But this was not the case with the IEP-11, consequently, IEP-11||$Ni(OH)_2$ in 1 M KOH still maintained very high areal capacity of 7.2 vs. 3.1 mAh cm^{-2} for PAQS||$Ni(OH)_2$ at 65 mg/cm^2, with only a 4 vs. 27% reduction in material activity compared to that in 10 M KOH. Furthermore, the trend in rate capability in 1 M KOH was similar to that in 10 M KOH, where IEP-11||$Ni(OH)_2$ retained higher capacity values at all the C-rates than that of PAQS||$Ni(OH)_2$ at both the anode mass loadings (Fig. S33).

2.4.5. *Self-discharge and float charge experiments*

Another important requisite that has to be positively evaluated (and neglected too in most of the reported literature) towards the commercialization of aqueous batteries comprising organic electrodes is their self-discharge and float charge behavior [62,63]. For these batteries, high self-discharge, potential instability, and high float charge capacity/current are the main drawbacks, which may decrease the cycle life under practical conditions. Once again, full cells with 10 M KOH electrolyte were tested for self-discharge and float charge behavior, which makes more sense because using lower electrolyte concentrations might result in obvious high self-discharge, and high irreversible capacity losses in the case of PAQS due to its inevitable solubility.

The self-discharge characteristic of PAQS||$Ni(OH)_2$ and IEP-11||$Ni(OH)_2$ was evaluated by interrupting galvanostatic cycling of the cells for different resting periods, i.e. 12, 24, 48, 96, and 192 h (see Fig. 7a and Fig. S35a and associated text in for detailed experimental protocol). Decay in open-circuit voltage (OCV) mAh/g; Fig. 7b) and capacity (Fig. 7c and Fig. S35b) was observed for both the cells, but this deterioration was more aggressive for PAQS||$Ni(OH)_2$. Furthermore, the recoverable capacity after self-discharge experiment was also prominent (more than 96% after 375 h of testing) for IEP-11||$Ni(OH)_2$, where in the case of PAQS||$Ni(OH)_2$, continuous irreversible capacity losses resulted in lower capacity recovery values (Fig. S34c).

The float charge current test is another important parameter to evaluate the stability and self-discharge behavior of batteries. These batteries have been charged to 100% state-of-charge (SOC) at 1.5 V and, then they are float charged at this voltage for different charging periods (from 1 to 192 h; see Fig. 7d and Fig. S36a and associated text in for detailed experimental protocol). The recorded currents under charge float conditions are called the float charge currents, which can be used to evaluate the energies required to keep the batteries at 100% SOC. The charging currents drop quickly when the float test is started for IEP-11||$Ni(OH)_2$ and subsequently become stable after a few hours. On the contrary, highly unstable currents with varied fluctuations, probably due to shuttle effect were noted for PAQS||$Ni(OH)_2$. Fig. 7e shows the measured float current drop, inferring relatively lower float charge current density values for IEP-11||$Ni(OH)_2$ than the PAQS||$Ni(OH)_2$. This suggests that the battery with IEP-11 anode possesses better float charge performance owing to the fact that it would require less energy to compensate for self-discharge or energy runaway or unstable of electrode materials than with PAQS anode [64]. Even more interestingly, the float charge capacity loss (the ratio of float charge capacity to the discharge capacity) trend was opposite to each other (Fig. 7f and Fig. S36b). Upon float charge, the loss of capacity was positive, and even significant (as high as ~10%, just after a short float charge period of 10 h) in the case of PAQS||$Ni(OH)_2$. This indicates the inadequacy of float charge conditions to compensate the self-discharge arising from irreversible capacity losses (dissolution of reduced anthraquinone species into the electrolyte, when the cell is charged) with PAQS anode. On the contrary, gain in the capacity (negative float charge capacity loss values), probably due to more activation of redox units upon float charge was observed

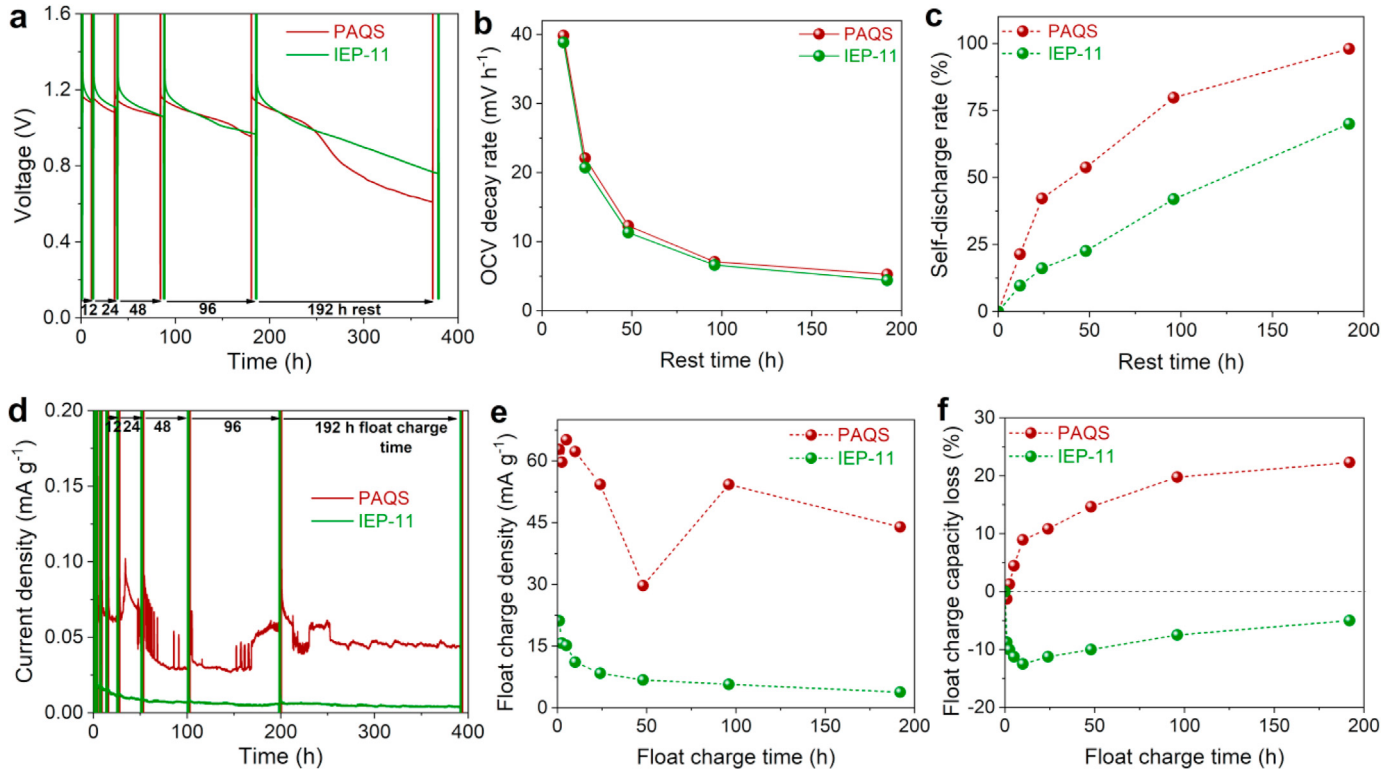

Fig. 7. Comparative self-discharge and float charge experiments at different resting and floating times, respectively for PAQS || $Ni(OH)_2$ and IEP-11 || $Ni(OH)_2$ full cells in 10 M KOH. a–c) self-discharge: voltage–time profiles (a), OCV decay rate (b) and self-discharge rate (c) at different resting time. d–f) Float charge: current density–time profiles (d), float charge density (e) and float charge capacity loss (f) at different float charge time.

under similar float charge conditions with IEP-11 anode. Furthermore, the capacity recovery after float charge experiment follows the same trend as of self-discharge experiments, and comparatively higher recoverable capacities was recorded with IEP-11||$Ni(OH)_2$ over PAQS||$Ni(OH)_2$ (Fig. S36c). Therefore, near-quantitative capacity recovery after self-discharge and float charge tests and gain in discharge capacity during the float charge with the porous polymer clearly specify reversible capacity losses upon self-discharge, while poor capacity recovery and loss of capacity during the same tests conclude the irreversible losses associated with the active-material dissolution in the case of linear polymer.

2.4.6. Polymer morphology–electrochemical properties–battery performance relationship

The following enhanced electrochemical performance for IEP-11||$Ni(OH)_2$ over PAQS||$Ni(OH)_2$ should be attributed to the intrinsic structure/morphology of the porous vs. linear polymer architectures:

i) Cycle stability: the robust and mechanically stable 3D architecture of the porous polymer rendered high structural, chemical, and dimensional integrity to the polymer electrode, thus enabling good cycling stability even in 1 M KOH. The shape-persistent, highly cross-linked covalent microporous polymeric nature of redox-active conjugated microporous polymers (RCMPs) was primarily credited for these excellent stabilities since this has been demonstrated to serve as a buffer to alleviate the structural strain during cycling while rendering high (electro)chemical stabilities to the redox centers inhibiting the dissolution of the active-moieties [44,45,48,49], even though more corroding higher electrolyte concentrations (>10 M) only helps to mitigate the dissolution of classical linear polymers, it cannot be completely alleviated, and therefore, advanced polymer architectures are still necessary to address this, of which we have illustrated an important example;

ii) Rate performance: the improved rate performance of IEP-11||$Ni(OH)_2$ over PAQS||$Ni(OH)_2$ not only at ambient temperature, but also at lower temperatures and with higher anode mass loading electrodes is due to the higher capacitive-limited capacity contributions (as revealed from power law, normalized capacity vs. $v^{-1/2}$ and Bode plot analyses) on account of more surface electrochemical reaction sites (high BET specific surface area) and short diffusion paths for ion/electron transport (mixed micro/mesoporosity), leading to the faster redox reactions (higher k^0), lower K^+ ion diffusion limitations in the bulk of the electrode (higher K^+ diffusivity) and accelerated relaxation (shorter τ_0) for porous polymer over linear one;

iii) Low-temperature operativity: the enhanced textural properties of porous polymer, along with its robust structure conferred superior capacity utilization and excellent low-temperature-resilient features over linear one;

iv) High mass loading electrodes: the optimum electronic/ionic conduction of our hybrid microporous polymer hold a great prospect to prepare high mass loading electrodes; most often, electron and/or ion diffusion limitations within the bulk of thick electrodes limit capacity utilization ratio; enthusiastically, our IEP-11 preserve excellent active-material utilization even in electrodes with very high mass loadings, resulting in high areal capacity output;

v) Low self-discharge and excellent float charge performance: once again, excellent stability of porous polymer due to its

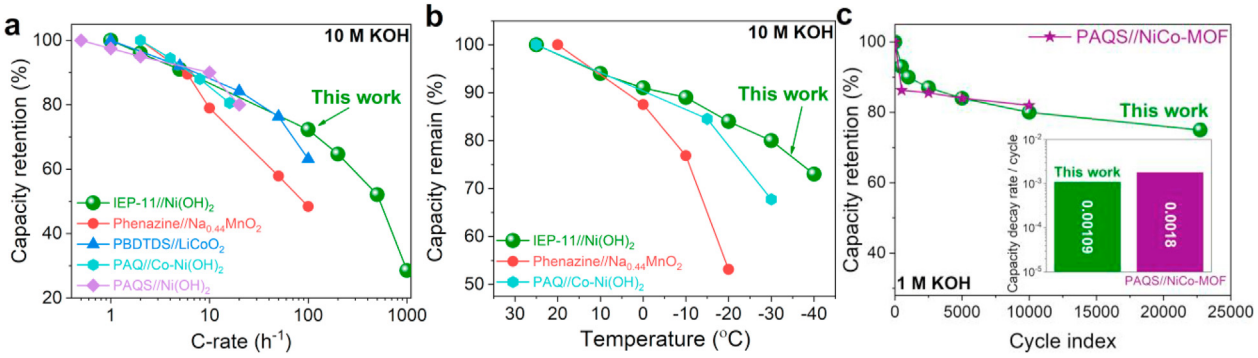

Fig. 8. Comparing IEP-11 || Ni(OH)$_2$ full cell performances with the state-of-the-art organic || Ni/Co/Mn based ARBs. a) Rate performance at ambient temperature in 10 M KOH. b) Low temperature operatively in 10 M KOH, depicting relative capacity retention at different temperatures w.r.t. the capacity at the highest temperature. c) Cycling performance in 1 M KOH showing % capacity retention against cycle index, and capacity decay rate per cycle (in logarithmic scale) is shown in the inset.

robust structure conferred low self-discharge and good float charge performance to the IEP-11||Ni(OH)$_2$, while unavoidable irreversible capacity losses associated with the active-material dissolution in the case of linear polymer rendered high self-discharge and poor float charge performance for PAQS||Ni(OH)$_2$.

2.5. IEP-11||Ni(OH)$_2$ vs. state-of-the-art ARBs

The full cell performance of IEP-11||Ni(OH)$_2$ in 1/10 M KOH aqueous electrolyte is compared with the state-of-the-art ARBs, containing small organic molecule or redox-active polymer anode and Ni/Co/Mn-based cathodes (Table S1). However, this comparison is not very straight forward always as not only because of different active-material mass loadings, electrode compositions and electrolyte concentrations employed in the literature, but also different applied electrochemical testing protocols. Whenever, similar experimental conditions are available, we compared IEP-11||Ni(OH)$_2$ performance with the state-of-the-art.

First, the remarkable rate performance (Fig. 8a) and notable low temperature performance (Fig. 8b) of IEP-11||Ni(OH)$_2$ in 10 M KOH were superior to the most of reported ARBs. Second, the outstanding cycling stability of IEP-11||Ni(OH)$_2$ in 1 M KOH was compared with PAQS||NiCo-MOF [20]. Though this latter cell demonstrated very good long-term cycle stability that retained 82% of its initial capacity over 10,000 cycles, longer cycling was not reported (Fig. 8c). Note, that this is the only report in literature where PAQS was successfully tested in 1 M KOH (contrary to other many articles were solubility issues of PAQS were evidenced that are in good agreement with the results of this work), but applied PAQS strategy prior to cycling before assembling into the full cell, and therefore, fair comparison cannot be accomplished, nonetheless given for the sake of reference. Remarkably, our IEP-11||Ni(OH)$_2$ was subjected to much extended cycling test over an extended period of 40 days that encompassed 22,730 cycles at 20C, exhibiting an outstanding 73% capacity retention. Consequently, an extremely low capacity decay rate of 0.00109% per cycle that is at least 0.6-fold higher than the PAQS||NiCo-MOF was demonstrated (Fig. 8c inset). Finally, hybridization and buckypaper strategy enabled us to push the polymer mass loading to a high value (65 mg/cm^2), and subsequently, competitive areal capacity of 7.6 mAh/cm^2 attained, which is, to the best of our knowledge, the highest value reported till date for organic cathodes in ARBs. This high value of areal capacity is particularly encouraging from the perspective reducing the cost of a practical battery by simultaneously minimizing the inactive components in the battery and maximizing the capacity at the cell level.

3. Conclusion

In conclusion, we successfully demonstrated a significantly improved alkaline rechargeable battery by enthusiastically incorporating anthraquinone redox units in the conjugated microporous polymer (IEP-11) structure. The electrochemical performance of our advanced IEP-11||commercial Ni(OH)$_2$ was compared with conventional linear PAQS||Ni(OH)$_2$, revealing superior performance in terms of concurrent cyclability, rate capability, low temperature performance, propensity to prepare high mas loading electrodes, self-discharge and float-charge characteristics in the commonly used high KOH concentrated electrolyte (*ca.*, 10 M). Also, IEP-11||Ni(OH)$_2$ overall performance was far superior to the reported organic||Ni/Co/Mn ARBs. But more importantly and for the first time, we demonstrated applicability of much lower KOH concentration (*ca.*, 1 M) with IEP-11 anode without compromising electrochemical performance with high cell voltage (0.98 V), high specific capacity (150 mAh/g at 1C), long cycle life (up to 22,730 cycles/960 h, with 75% capacity retention at 20C), excellent rate performance (75 mAh/g at 50C) and low temperature operativity (75 mAh/g at −10 °C).

This enhanced electrochemical performance for IEP-11||Ni(OH)$_2$ over PAQS||Ni(OH)$_2$ was attributed to the intrinsic structure/morphology of the porous vs. linear polymer architectures: (1) the robust and mechanically stable 3D architecture of the porous polymer enabled impressive cycling stability even in 1 M KOH; (2) the mixed micro-/mesoporosity and high BET specific surface area rendered superior rate capability with higher anode mass loading electrodes at ambient and also low temperatures; and (3) the robust porous structure once again conferred low self-discharge and good float charge performances. We hypothesize that the presented approach not only paves ways toward the design of 'high-performance' and 'advanced' alkaline rechargeable batteries, but also may presumably leads to the development of safe, environmentally benign, and practical organic batteries by taking advantage of the commercially matured Ni-based cathode, the high safety of less corroding 1 M KOH aqueous electrolyte, and the presumably economical and sustainable ultrarobust organic anode.

CRediT authorship contribution statement

Rebecca Grieco: Data curation, Investigation, Methodology, Writing – original draft.

Antonio Molina: Conceptualization, Data curation, Investigation, Methodology, Writing – original draft.

Jaime S Sanchez: Data curation, Investigation, Methodology.

Nagaraj Patil: Conceptualization, Funding acquisition, Data curation, Investigation, Methodology, Writing – original draft, Writing – review & editing.

Marta Liras: Writing – review & editing.

Rebeca Marcilla: Funding acquisition, Writing – review & editing, Project administration, Supervision.

Declaration of competing interest

The authors declare that they have no known competing financial interests or personal relationships that could have appeared to influence the work reported in this article.

Acknowledgments

The authors thank the Spanish Ministry of Science, Innovation and Universities through the SUSBAT project (Ref. RTI2018-101049-B-I00) (MINECO/FEDER, UE) for financial supports. NP and ML also appreciates Spanish MINECO and European Social Fund for the Juan de la Cierva-formation fellowship [FJC2018-037781-I] and the Ramón y Cajal contract (RyC-2015-18677). The authors also thank the European Union's Horizon 2020 research and innovation programme under the Marie Skłodowska-Curie Grant agreement (Grant No 860403).

Appendix A. Supplementary data

Supplementary data to this article can be found online at https://doi.org/10.1016/j.mtener.2022.101014.

References

[1] M. Armand, J.-M. Tarascon, Building better batteries, Nature. 451 (2008) 652–657, https://doi.org/10.1038/451652a.
[2] D. Larcher, J.-M. Tarascon, Towards greener and more sustainable batteries for electrical energy storage, Nat. Chem. 7 (2015) 19–29, https://doi.org/10.1038/nchem.2085.
[3] S. Chu, Y. Cui, N. Liu, The path towards sustainable energy, Nat. Mater. 16 (2017) 16–22, https://doi.org/10.1038/nmat4834.
[4] D. Chao, W. Zhou, F. Xie, C. Ye, H. Li, M. Jaroniec, S.-Z. Qiao, Roadmap for advanced aqueous batteries: from design of materials to applications, Sci. Adv. 6 (2020), eaba4098, https://doi.org/10.1126/sciadv.aba4098.
[5] J. Shin, J.W. Choi, Opportunities and reality of aqueous rechargeable batteries, Adv. Energy Mater. 10 (2020) 2001386, https://doi.org/10.1002/aenm.202001386.
[6] M. Perrin, Y.M. Saint-Drenan, F. Mattera, P. Malbranche, Lead–acid batteries in stationary applications: competitors and new markets for large penetration of renewable energies, J. Power Sources 144 (2005) 402–410, https://doi.org/10.1016/j.jpowsour.2004.10.026.
[7] T.-K. Ying, X.-P. Gao, W.-K. Hu, F. Wu, D. Noréus, Studies on rechargeable NiMH batteries, Int. J. Hydrogen Energy 31 (2006) 525–530, https://doi.org/10.1016/j.ijhydene.2005.04.018.
[8] D. Pavlov, R. Popova, Mechanism of passivation processes of the lead sulphate electrode, Electrochim. Acta 15 (1970) 1483–1491, https://doi.org/10.1016/0013-4686(70)80069-X.
[9] S.R. Ovshinsky, M.A. Fetcenko, J. Ross, A nickel metal hydride battery for electric vehicles, Science 260 (1993) 176–181, https://doi.org/10.1126/science.260.5105.176.
[10] H. Wang, R. Tan, Z. Yang, Y. Feng, X. Duan, J. Ma, Stabilization perspective on metal anodes for aqueous batteries, Adv. Energy Mater. 11 (2021) 2000962, https://doi.org/10.1002/aenm.202000962.
[11] J. Xie, Q. Zhang, Recent progress in multivalent metal (Mg, Zn, Ca, and Al) and metal-ion rechargeable batteries with organic materials as promising electrodes, Small 15 (2019) 1805061, https://doi.org/10.1002/smll.201805061.
[12] C. Han, J. Zhu, C. Zhi, H. Li, The rise of aqueous rechargeable batteries with organic electrode materials, J. Mater. Chem. A. 8 (2020) 15479–15512, https://doi.org/10.1039/D0TA03947K.
[13] J. Huang, X. Dong, Z. Guo, Y. Wang, Progress of organic electrodes in aqueous electrolyte for energy storage and conversion, Angew. Chem. Int. Ed. 59 (2020) 18322–18333, https://doi.org/10.1002/anie.202003198.
[14] Z. Song, H. Zhou, Towards sustainable and versatile energy storage devices: an overview of organic electrode materials, Energy Environ. Sci. 6 (2013) 2280–2301, https://doi.org/10.1039/c3ee40709h.
[15] T.B. Schon, B.T. McAllister, P.-F. Li, D.S. Seferos, The rise of organic electrode materials for energy storage, Chem. Soc. Rev. 45 (2016) 6345–6404, https://doi.org/10.1039/C6CS00173D.
[16] S. Lee, J. Hong, K. Kang, Redox-active organic compounds for future sustainable energy storage system, Adv. Energy Mater. 10 (2020) 2001445, https://doi.org/10.1002/aenm.202001445.
[17] K. Lin, R. Gómez-Bombarelli, E.S. Beh, L. Tong, Q. Chen, A. Valle, A. Aspuru-Guzik, M.J. Aziz, R.G. Gordon, A redox-flow battery with an alloxazine-based organic electrolyte, Nat. Energy 1 (2016) 16102, https://doi.org/10.1038/nenergy.2016.102.
[18] Y. Liang, Y. Jing, S. Gheytani, K.-Y. Lee, P. Liu, A. Facchetti, Y. Yao, Universal quinone electrodes for long cycle life aqueous rechargeable batteries, Nat. Mater. 16 (2017) 841–848, https://doi.org/10.1038/nmat4919.
[19] E. Dražević, A.S. Andersen, K. Wedege, M.L. Henriksen, M. Hinge, A. Bentien, Investigation of low-cost oligoanthraquinones for alkaline, aqueous rechargeable batteries with cell potential up to 1.13 V, J. Power Sources 381 (2018) 94–100, https://doi.org/10.1016/j.jpowsour.2018.01.092.
[20] J. Li, H. Zhao, J. Wang, N. Li, M. Wu, Q. Zhang, Y. Du, Interplanar space-controllable carboxylate pillared metal organic framework ultrathin nanosheet for superhigh capacity rechargeable alkaline battery, Nano Energy 62 (2019) 876–882, https://doi.org/10.1016/j.nanoen.2019.06.009.
[21] C. Liu, T. Ma, K. Xia, X. Hou, Q. Nian, Y. Cai, J. Liang, High performance polyanthraquinone/Co–Ni$(OH)_2$ aqueous batteries based on hydroxyl and potassium insertion/extraction reactions, Sustain. Energy Fuels 4 (2020) 132–137, https://doi.org/10.1039/C9SE00598F.
[22] T. Sun, C. Liu, J. Wang, Q. Nian, Y. Feng, Y. Zhang, Z. Tao, J. Chen, A phenazine anode for high-performance aqueous rechargeable batteries in a wide temperature range, Nano Res. 13 (2020) 676–683, https://doi.org/10.1007/s12274-020-2674-3.
[23] Y. Jing, Y. Liang, S. Gheytani, Y. Yao, A quinone anode for lithium-ion batteries in mild aqueous electrolytes, ChemSusChem 13 (2020) 2250–2255, https://doi.org/10.1002/cssc.202000094.
[24] P. Novák, K. Müller, K.S.V. Santhanam, O. Haas, Electrochemically active polymers for rechargeable batteries, Chem. Rev. 97 (1997) 207–282, https://doi.org/10.1021/cr941181o.
[25] S. Muench, A. Wild, C. Friebe, B. Häupler, T. Janoschka, U.S. Schubert, Polymer-based organic batteries, Chem. Rev. 116 (2016) 9438–9484, https://doi.org/10.1021/acs.chemrev.6b00070.
[26] J. Kim, J.H. Kim, K. Ariga, Redox-active polymers for energy storage nanoarchitectonics, Joule 1 (2017) 739–768, https://doi.org/10.1016/j.joule.2017.08.018.
[27] K. Hatakeyama-Sato, T. Nagano, S. Noguchi, Y. Sugai, J. Du, H. Nishide, K. Oyaizu, Hydrophilic organic redox-active polymer nanoparticles for higher energy density flow batteries, ACS Appl. Polym. Mater. 1 (2019) 188–196, https://doi.org/10.1021/acsapm.8b00074.
[28] Y. Chen, S. Zhuo, Z. Li, C. Wang, Redox polymers for rechargeable metal-ion batteries, Energy 2 (2020) 100030, https://doi.org/10.1016/j.enchem.2020.100030.
[29] N. Goujon, N. Casado, N. Patil, R. Marcilla, D. Mecerreyes, Organic batteries based on just redox polymers, Prog. Polym. Sci. 122 (2021) 101449, https://doi.org/10.1016/j.progpolymsci.2021.101449.
[30] K. Oyaizu, W. Choi, H. Nishide, Functionalization of poly(4-chloromethylstyrene) with anthraquinone pendants for organic anode-active materials, Polym. Adv. Technol. 22 (2011) 1242–1247, https://doi.org/10.1002/pat.1968.
[31] W. Choi, D. Harada, K. Oyaizu, H. Nishide, Aqueous electrochemistry of poly(vinylanthraquinone) for anode-active materials in high-density and rechargeable polymer/air batteries, J. Am. Chem. Soc. 133 (2011) 19839–19843, https://doi.org/10.1021/ja206961t.
[32] K. Oyaizu, Y. Niibori, A. Takahashi, H. Nishide, BODIPY-sensitized photocharging of anthraquinone-populated polymer layers for organic photorechargeable air battery, J. Inorg. Organomet. Polym. Mater. 23 (2013) 243–250, https://doi.org/10.1007/s10904-012-9751-3.
[33] T. Kawai, K. Oyaizu, H. Nishide, High-density and robust charge storage with poly(anthraquinone-substituted norbornene) for organic electrode-active materials in polymer–air secondary batteries, Macromolecules 48 (2015) 2429–2434, https://doi.org/10.1021/ma502396r.
[34] Y. Li, L. Liu, C. Liu, Y. Lu, R. Shi, F. Li, J. Chen, Rechargeable aqueous polymer-air batteries based on polyanthraquinone anode, Inside Chem. 5 (2019) 2159–2170, https://doi.org/10.1016/j.chempr.2019.06.001.
[35] Y. Yusran, Q. Fang, V. Valtchev, Electroactive covalent organic frameworks: design, synthesis, and applications, Adv. Mater. 32 (2020) 2002038, https://doi.org/10.1002/adma.202002038.
[36] J. Li, X. Jing, Q. Li, S. Li, X. Gao, X. Feng, B. Wang, Bulk COFs and COF nanosheets for electrochemical energy storage and conversion, Chem. Soc. Rev. 49 (2020) 3565–3604, https://doi.org/10.1039/D0CS00017E.
[37] T. Sun, J. Xie, W. Guo, D.-S. Li, Q. Zhang, Covalent–organic frameworks: advanced organic electrode materials for rechargeable batteries, Adv. Energy Mater. 10 (2020) 1904199, https://doi.org/10.1002/aenm.201904199.
[38] X. Liu, C. Liu, W. Lai, W. Huang, Porous organic polymers as promising electrode materials for energy storage devices, Adv. Mater. Technol. 5 (2020) 2000154, https://doi.org/10.1002/admt.202000154.
[39] R. Iqbal, G. Yasin, M. Hamza, S. Ibraheem, B. Ullah, A. Saleem, S. Ali, S. Hussain, T. Anh Nguyen, Y. Slimani, R. Pathak, State of the art two-dimensional covalent organic frameworks: prospects from rational design and reactions to applications for advanced energy storage technologies, Coord. Chem. Rev. 447 (2021) 214152, https://doi.org/10.1016/j.ccr.2021.214152.

[40] C. Wei, L. Tan, Y. Zhang, K. Zhang, B. Xi, S. Xiong, J. Feng, Y. Qian, Covalent organic frameworks and their derivatives for better metal anodes in rechargeable batteries, ACS Nano 15 (2021) 12741–12767, https://doi.org/10.1021/acsnano.1c05497.
[41] J. Choi, J.H. Ko, C.W. Kang, S.M. Lee, H.J. Kim, Y.-J. Ko, M. Yang, S.U. Son, Enhanced redox activity of a hollow conjugated microporous polymer through the generation of carbonyl groups by carbonylative Sonogashira coupling, J. Mater. Chem. A. 6 (2018) 6233–6237, https://doi.org/10.1039/C8TA01379A.
[42] X.-C. Li, Y. Zhang, C.-Y. Wang, Y. Wan, W.-Y. Lai, H. Pang, W. Huang, Redox-active triazatruxene-based conjugated microporous polymers for high-performance supercapacitors, Chem. Sci. 8 (2017) 2959–2965, https://doi.org/10.1039/C6SC05532J.
[43] Y.-Y. Liu, X.-C. Li, S. Wang, T. Cheng, H. Yang, C. Liu, Y. Gong, W.-Y. Lai, W. Huang, Self-templated synthesis of uniform hollow spheres based on highly conjugated three-dimensional covalent organic frameworks, Nat. Commun. 11 (2020) 5561, https://doi.org/10.1038/s41467-020-18844-4.
[44] A. Molina, N. Patil, E. Ventosa, M. Liras, J. Palma, R. Marcilla, New anthraquinone-based conjugated microporous polymer cathode with ultra-high specific surface area for high-performance lithium-ion batteries, Adv. Funct. Mater. 30 (2020) 1908074, https://doi.org/10.1002/adfm.201908074.
[45] A. Molina, N. Patil, E. Ventosa, M. Liras, J. Palma, R. Marcilla, Electrode engineering of redox-active conjugated microporous polymers for ultra-high areal capacity organic batteries, ACS Energy Lett. 5 (2020) 2945–2953, https://doi.org/10.1021/acsenergylett.0c01577.
[46] W. Liu, X. Luo, Y. Bao, Y.P. Liu, G.-H. Ning, I. Abdelwahab, L. Li, C.T. Nai, Z.G. Hu, D. Zhao, B. Liu, S.Y. Quek, K.P. Loh, A two-dimensional conjugated aromatic polymer via C–C coupling reaction, Nat. Chem. 9 (2017) 563–570, https://doi.org/10.1038/nchem.2696.
[47] S.-Y. Li, W.-H. Li, X.-L. Wu, Y. Tian, J. Yue, G. Zhu, Pore-size dominated electrochemical properties of covalent triazine frameworks as anode materials for K-ion batteries, Chem. Sci. 10 (2019) 7695–7701, https://doi.org/10.1039/C9SC02340B.
[48] L. Zhong, Z. Fang, C. Shu, C. Mo, X. Chen, D. Yu, Redox donor–acceptor conjugated microporous polymers as ultralong-lived organic anodes for rechargeable air batteries, Angew. Chem. Int. Ed. 60 (2021) 10164–10171, https://doi.org/10.1002/anie.202016746.
[49] Z. Zhao-Karger, P. Gao, T. Ebert, S. Klyatskaya, Z. Chen, M. Ruben, M. Fichtner, New organic electrode materials for ultrafast electrochemical energy storage, Adv. Mater. 31 (2019) 1806599, https://doi.org/10.1002/adma.201806599.
[50] G. Nikiforidis, M. Raghibi, A. Sayegh, M. Anouti, Low-concentrated lithium hexafluorophosphate ternary-based electrolyte for a reliable and safe NMC/graphite lithium-ion battery, J. Phys. Chem. Lett. 12 (2021) 1911–1917, https://doi.org/10.1021/acs.jpclett.0c03736.
[51] Z. Mao, R.E. White, The self-discharge of the NiOOH/$Ni(OH)_2$ electrode constant potential study, J. Electrochem. Soc. 139 (1992) 1282–1289, https://doi.org/10.1149/1.2069397.
[52] N. Vassal, E. Salmon, J.-F. Fauvarque, Nickel/metal hydride secondary batteries using an alkaline solid polymer electrolyte, J. Electrochem. Soc. 146 (1999) 20–26, https://doi.org/10.1149/1.1391558.
[53] N. Patil, A. Aqil, F. Ouhib, S. Admassie, O. Inganäs, C. Jérôme, C. Detrembleur, Bioinspired redox-active catechol-bearing polymers as ultrarobust organic cathodes for lithium storage, Adv. Mater. 29 (2017) 1703373, https://doi.org/10.1002/adma.201703373.
[54] N. Patil, C. Cruz, D. Ciurduc, A. Mavrandonakis, J. Palma, R. Marcilla, An ultrahigh performance zinc-organic battery using poly(catechol) cathode in $Zn(TFSI)_2$-based concentrated aqueous electrolytes, Adv. Energy Mater. (2021) 2100939, https://doi.org/10.1002/aenm.202100939.
[55] V. Augustyn, J. Come, M.A. Lowe, J.W. Kim, P.-L. Taberna, S.H. Tolbert, H.D. Abruña, P. Simon, B. Dunn, High-rate electrochemical energy storage through Li^+ intercalation pseudocapacitance, Nat. Mater. 12 (2013) 518–522, https://doi.org/10.1038/nmat3601.
[56] S. Park, Z. Khan, T.J. Shin, Y. Kim, H. Ko, Rechargeable Na/Ni batteries based on the $Ni(OH)_2$/NiOOH redox couple with high energy density and good cycling performance, J. Mater. Chem. A. 7 (2019) 1564–1573, https://doi.org/10.1039/C8TA10830G.
[57] A. Ahmad, A. Imani, L. Mao, R. Iqbal, H. Zhang, Z.A. Ghazi, R. Ahmad, A.A. Khan, L. Xie, C. Chen, Z. Zhang, Z. Wei, A bifunctional and free-standing organic composite film with high flexibility and good tensile strength for tribological and electrochemical applications, Adv. Mater. Technol. 4 (2019) 1900617, https://doi.org/10.1002/admt.201900617.
[58] R.J. Gilliam, J.W. Graydon, D.W. Kirk, S.J. Thorpe, A review of specific conductivities of potassium hydroxide solutions for various concentrations and temperatures, Int. J. Hydrogen Energy 32 (2007) 359–364, https://doi.org/10.1016/j.ijhydene.2006.10.062.
[59] F. Li, X. Hu, Zinc metal energy storage devices under extreme conditions of low temperatures, Batter. Supercaps. 4 (2021) 389–406, https://doi.org/10.1002/batt.202000243.
[60] Q. Nian, T. Sun, S. Liu, H. Du, X. Ren, Z. Tao, Issues and opportunities on low-temperature aqueous batteries, Chem. Eng. J. 423 (2021) 130253, https://doi.org/10.1016/j.cej.2021.130253.
[61] D.L. Wood, J. Li, C. Daniel, Prospects for reducing the processing cost of lithium ion batteries, J. Power Sources 275 (2015) 234–242, https://doi.org/10.1016/j.jpowsour.2014.11.019.
[62] J. Liu, C. Xu, Z. Chen, S. Ni, Z.X. Shen, Progress in aqueous rechargeable batteries, Green Energy Environ 3 (2018) 20–41, https://doi.org/10.1016/j.gee.2017.10.001.
[63] L. Droguet, A. Grimaud, O. Fontaine, J. Tarascon, Water-in-salt electrolyte (WISE) for aqueous batteries: a long way to practicality, Adv. Energy Mater. 10 (2020) 2002440, https://doi.org/10.1002/aenm.202002440.
[64] J. Zhi, A.Z. Yazdi, G. Valappil, J. Haime, P. Chen, Artificial solid electrolyte interphase for aqueous lithium energy storage systems, Sci. Adv. 3 (2017) e1701010, https://doi.org/10.1126/sciadv.1701010.